

Synchronization in a network of model neurons

Maruthi Pradeep Kanth Jampa,¹ Abhijeet R. Sonawane,² Prashant M. Gade,² and Sudeshna Sinha¹

¹*The Institute of Mathematical Sciences, CIT Campus, Taramani, Chennai 600 113, India*

²*Centre for Modeling and Simulation, University of Pune, Pune 411 007, India*

(Received 10 July 2006; revised manuscript received 9 October 2006; published 27 February 2007)

We study the spatiotemporal dynamics of a network of coupled chaotic maps modelling neuronal activity, under variation of coupling strength ϵ and degree of randomness in coupling p . We find that at high coupling strengths ($\epsilon > \epsilon_{\text{fixed}}$) the unstable saddle point solution of the local chaotic maps gets stabilized. The range of coupling where this spatiotemporal fixed point gains stability is unchanged in the presence of randomness in the connections, namely ϵ_{fixed} is invariant under changes in p . As coupling gets weaker ($\epsilon < \epsilon_{\text{fixed}}$), the spatiotemporal fixed point loses stability, and one obtains chaos. In this regime, when the coupling connections are completely regular ($p=0$), the network becomes spatiotemporally chaotic. Interestingly however, in the presence of random links ($p>0$) one obtains spatial synchronization in the network. We find that this range of synchronized chaos increases exponentially with the fraction of random links in the network. Further, in the space of fixed coupling strengths, the synchronization transition occurs at a *finite* value of p , a scenario quite distinct from the many examples of synchronization transitions at $p \rightarrow 0$. Further we show that the synchronization here is robust in the presence of parametric noise, namely in a network of nonidentical neuronal maps. Finally we check the generality of our observations in networks of neurons displaying both spiking and bursting dynamics.

DOI: [10.1103/PhysRevE.75.026215](https://doi.org/10.1103/PhysRevE.75.026215)

PACS number(s): 05.45.-a

I. INTRODUCTION

One of the important prototypes of complex phenomena are systems composed of large numbers of low dimensional nonlinear dynamical units. The basic ingredients of such systems are (i) creation of local chaos or local instability by a low dimensional mechanism and (ii) spatial transmission of energy and information by coupling connections of varying strengths and underlying topologies.

The central question of interest here is the following: how do collections of entities which display complex chaotic behavior when isolated (such as cardiac or neuronal cells) manage to yield coherent regular behavior when coupled. It is known that diffusive coupling regularizes spatiotemporal dynamics of coupled chaotic systems [1,2]. Here we demonstrate another mechanism for inducing regular spatiotemporal dynamics: the presence of random nonlocal coupling.

We focus on the coupled map lattice (CML), which is a model capturing the essential features of nonlinear dynamics of extended systems [1]. This model is defined on a lattice, the dynamics of whose nodes is given by a local (commonly nonlinear) map. Over the past decade, research centered around CML has yielded suggestive conceptual models of spatiotemporal phenomena, in fields ranging from biology to engineering. In particular, this class of systems is of considerable interest in modelling phenomena as diverse as Josephson junction arrays, multimode lasers, vortex dynamics, and even evolutionary biology. The ubiquity of distributed complex systems has made the CML a focus of sustained research interest.

A very well-studied coupling form in CMLs is nearest neighbor coupling. While this regular network is the chosen topology of innumerable studies, there are strong reasons to revisit this fundamental issue in the light of the fact that some degree of randomness in spatial coupling can be closer to physical reality than strict nearest neighbor scenarios. In fact, many systems of biological, technological, and physical

significance are better described by randomizing some fraction of the regular links [3–7]. So here we will study the spatiotemporal dynamics of a CML of relevance to biology, with some of its coupling connections rewired randomly, i.e., an extended system comprised of a collection of complex elemental dynamical units with varying degrees of randomness in its spatial connections.

In the context of synchronization [8], it has recently been found that random coupling yields spatiotemporal synchronization in a network of chaotic one-dimensional local maps [9]. That is, the strongly unstable fixed point of the local maps (such as logistic, circle and tent maps) were stabilized under increasing randomness in the coupling connections. Thus interestingly, the inherent chaos present in the individual local units is suppressed by the coupling, giving way to a stable global attractor. Further, the range of stability of this spatiotemporal fixed point increased monotonically with increasingly random coupling [10].

In this work we will study a network of model neurons, and try to discern the effect of random coupling on the spatiotemporal dynamics. Note that there have been many studies on coupled one-dimensional maps [1,9]. However the dynamics of coupled higher dimensional maps could be qualitatively different, and they may display certain behaviors that are not obtained in one-dimensional maps. There has been considerable success in realistically modelling neurons [11,12] and lasers [13] by higher dimensional maps. Thus studying coupled systems of higher dimensional maps could be more relevant for practical applications.

The primary questions we address here are the following:

- (i) Does random coupling enhance the parameter region yielding a stable global fixed point?
- (ii) Does random coupling yield spatial synchronization?
- (iii) How do the synchronization properties change with respect to increasing randomness? The issue here is the following: is there some optimal value of randomness for ob-

taining dynamical regularity and/or synchronization, or is this a monotonic function of some measure of the randomness, interpolating smoothly between the regular and random limits [14].

(iv) Does the synchronization transition occur when we have a finite fraction of random nonlocal connections? This question is significant in the following context: while there is much evidence that random nonlocal connections, even in a small fraction, makes a big difference to geometrical properties like characteristic path length, its implications for dynamics is still unclear and even conflicting. So it is important to determine what dynamical changes occur at very low values of disorder, namely does the behavior change as soon as nonlocal shortcuts are put in place (as observed in equilibrium models [5]), or do the transitions occur at significantly higher degrees of disorder.

(v) Is the synchronization robust with respect to parametric noise, namely is it present in networks of nonidentical components (albeit in a weaker form)?

In this work we will probe all the above issues. In the sections below, we will first describe the model in detail, and then we will present the results and conclude with a summary and discussions.

II. NETWORK OF MODEL NEURONS

Here we consider a one-dimensional ring of neurons modelled by maps. In certain parameter regimes this neuronal map exhibits chaotic behavior about one of its fixed points. In our system the local model neurons operate in this chaotic regime, and we will show the transition of such chaotic maps to a synchronized state, under varying coupling strengths and randomness in coupling connections.

Specifically, our local dynamical unit is the two-dimensional model neuron map, proposed by Chialvo [11]. This map determines the local dynamics in our network, and is given as

$$\begin{aligned} x_{n+1} &= f_1(x_n, y_n) = x_n^2 \exp(y_n - x_n) + k, \\ y_{n+1} &= f_2(x_n, y_n) = ay_n - bx_n + c, \end{aligned} \quad (1)$$

where n is discrete time.

As appropriate in the context of excitable biological systems, here x_n is the activation variable (analogous to membrane potential) and y_n is the recovery variable [11].

Parameter a is the rate constant for y_n and b is the activation dependence of the recovery variable (as it relates y_n to x_n). Parameters k and c are offsets to the x_n and y_n variables, respectively. In this work we choose the parameter values $a=0.89, b=0.18, c=0.28$.

The *nullclines* of this neuronal system are given by, $x_{n+1} = x_n$ leading to

$$x^* = x^{*2} \exp(y^* - x^*) + k, \quad (2)$$

and $y_{n+1} = y_n$ leading to

$$y^* = ay^* - bx^* + c, \quad (3)$$

whose simultaneous solution gives

$$y^* = \ln x^* - k - 2 \ln x^* + x^*, \quad (4)$$

$$y^* = \frac{c - bx^*}{1 - a}. \quad (5)$$

When $k \sim 0.03$, this map has very interesting dynamics. Here, the phase flow spirals towards the fixed point $\sim (1, 1)$ and then suddenly bursts out. This leads to chaotic spiking behavior about the saddle node. We use this regime for our local dynamics.

When these neuronal maps are coupled to nearest neighbors through the x variable (namely the membrane potential), the dynamics of the network is given as

$$\begin{aligned} x_{n+1}(i) &= (1 - \epsilon)f_1[x_n(i), y_n(i)] + \frac{\epsilon}{2}\{g[x_n(i+1)] + g[x_n(i-1)]\}, \\ y_{n+1}(i) &= f_2[x_n(i), y_n(i)], \end{aligned} \quad (6)$$

where index n denotes iteration steps and i is the site index on the lattice with periodic boundary conditions. Here $f_1(x, y)$ and $f_2(x, y)$ are given by the local evolution map at each site [Eqs. (1)]. The coupling function $g(x)$ can take different forms. In this work we use the linear coupling form $g(x) = x$. The parameter ϵ gives the coupling strength.

Now on this regular lattice we introduce varying degrees of randomness, namely we introduce some fraction of random links replacing the regular nearest neighbor connections. This mimics real life situations in which nonlocal connections exist along with predominantly local ones [15].

The evolution is given by

$$\begin{aligned} x_{n+1}(i) &= (1 - \epsilon)f_1[x_n(i), y_n(i)] + \frac{\epsilon}{2}\{g[x_n(\xi)] + g[x_n(\eta)]\}, \\ y_{n+1}(i) &= f_2[x_n(i), y_n(i)], \end{aligned} \quad (7)$$

where $\xi = i+1$ with probability $1-p$ and is a randomly chosen integer such that $1 \leq \xi \leq N$ with probability p . Similarly $\eta = i-1$ with probability $1-p$ and is a randomly chosen integer such that $1 \leq \eta \leq N$ with probability p . In this work, ξ and η are chosen randomly at every time step. This is unlike the case of quenched randomness, more usually studied in literature, where ξ and η do not change in time. Clearly the $p=0$ case corresponds to regular nearest neighbor coupling and $p=1$ to completely random connections. This scenario is much like small world networks at low p , namely $p \rightarrow 0$. Note however that we explore the full range of p ($0 \leq p \leq 1$) here. So the study is inclusive of, but not confined to, small world networks. As mentioned above, the connections are rewired *dynamically* and we are not using quenched randomness here. Rather the network *switches the random links* from time to time.

The focus of this work is to determine what dynamical properties are significantly affected by the way connections are made between elements. We present our results below.

III. RESULTS FOR HOMOGENEOUS NETWORKS

Now we numerically examine the phenomenology of this network of neurons under variation of coupling strengths and degrees of randomness in coupling. The spatiotemporal pat-

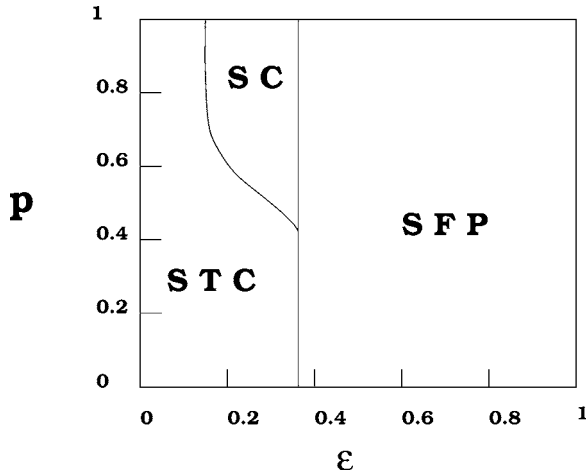


FIG. 1. We plot the phase diagram of coupled Chialvo maps in the two parameter space of coupling strength ϵ and rewiring probability p . The abbreviation SC, STC, and SFP denote synchronized chaos, spatiotemporal chaos, and synchronized fixed point, respectively.

terns of this network are clearly evident from the phase diagram displayed in Fig. 1 [16] and the bifurcation diagrams in Fig. 2. The following are the salient features of this system.

Regularity at high coupling strengths. The chaotic spiking behavior of the local maps occurs about the saddle fixed point at $\approx(1, 1)$. Under strong coupling this fixed point becomes a *stable global attractor*. That is, when the coupling strengths are in the range $\epsilon_{\text{fixed}} < \epsilon \leq 1$ ($\epsilon_{\text{fixed}} \sim 0.361$), the dynamics of the network is attracted to the spatiotemporal fixed point: $x_n(i)=1, y_n(i)=1$, for all i and n (see Fig. 2). Note that the value of ϵ_{fixed} observed numerically matches that obtained analytically in the section above.

For coupling strengths smaller than ϵ_{fixed} , the spatiotemporal fixed point loses stability. For regular coupling one then obtains spatiotemporal chaos. However if there is some degree of randomness in the coupling connections (namely $p > 0$), one obtains ranges of coupling strengths ($\epsilon_{\text{sync}} < \epsilon < \epsilon_{\text{fixed}}$) where *spatial synchronization* occurs. This is evident through Fig. 2 displaying the *spatial pattern* obtained for different coupling strengths, for different degrees of random coupling p . These bifurcation diagrams display the state of all the sites at a given instant of time, and it clearly shows that $p > 0$ opens up a window of coupling strengths where spatial synchronization occurs, i.e., all nodes in the network have the same state, seen simply as a point in the bifurcation diagram.

Also note that the randomly rewired network has large spikes in the temporal evolution of the membrane potential, as compared to the regular ring of model neurons (see Fig. 3).

We study the degree of synchronization in the systems quantitatively through an average error function defined as

$$Z(n) = \frac{1}{N} \sum_{i=0}^N [x_n(i) - x_n(N/2)]^2 \quad (8)$$

averaged over time n and over different initial realizations of the network. Figs. 4 and 5 display this quantity for different

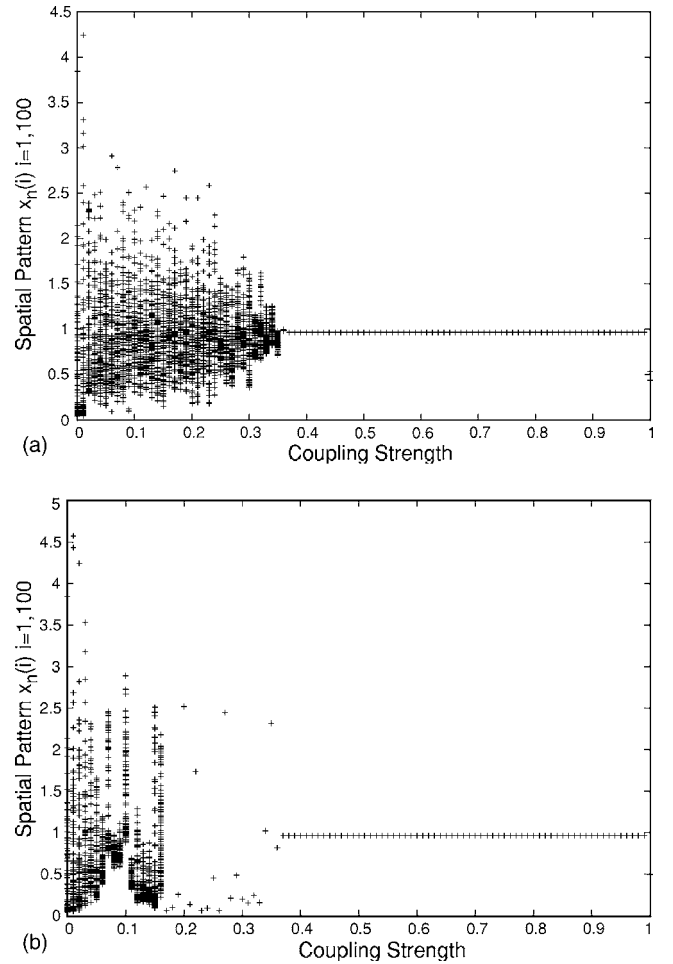


FIG. 2. Bifurcation diagrams of the spatial pattern in the network, at an instant of time (after transience), with respect to coupling strength ϵ , with fraction of random links $p=0$ (top) and $p=1$ (bottom).

rewiring probabilities and different coupling strengths. $\langle Z \rangle = 0$ indicates complete synchronization.

It is evident from Fig. 4 that the transition to synchronization occurs at coupling strengths higher than ϵ_{sync} . It is clear that for higher p , ϵ_{sync} is lower. So random links in the network enhance the range of synchronization.

Figure 5 shows the average synchronization error for a fixed coupling strength, with respect to varying p . Clearly the transition to synchronization occurs at a *finite* p_{sync} , with the value of p_{sync} decreasing with increasing coupling strengths ($p_{\text{sync}} \sim 0.4$ at $\epsilon=0.3$ in Fig. 5). This is quite distinct from $p \rightarrow 0$ synchronization transitions observed in many systems [5,17]. Thus one obtains long-range order only at some finite degree of disorder p in the coupling connections.

Further, study of the window of synchronized chaos, $R = \epsilon_{\text{fixed}} - \epsilon_{\text{sync}}$, shows that the range of synchronization increases *monotonically* with the fraction of random links p (see Fig. 6). The functional dependence of this range R on p is exponential over a large range ($0.1 < p \sim 0.8$), with saturation occurring at $p \rightarrow 1$. For $p=0$, the links will be completely local and synchronized chaos cannot exist. Thus for very small values of p , we see that the range goes to zero con-

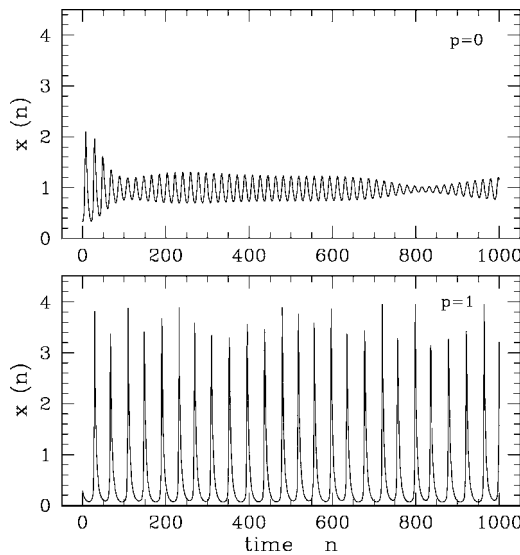


FIG. 3. Time series of a representative model neuron in a network with (i) $p=0$ (upper panel) and (ii) $p=1$ (lower panel). Coupling strength $\epsilon=0.3$ here. It is evident that random networks yield large spikes in the membrane potential, as compared to the regular ring of model neurons.

tinuously. Our study then indicates that synchronization properties interpolate smoothly between the limits of regular and random connections without in any sense being “optimal” or more pronounced at some intermediate (low) value of p [14].

Also note that coupling through such dynamically updated random links is effectively similar to global coupling

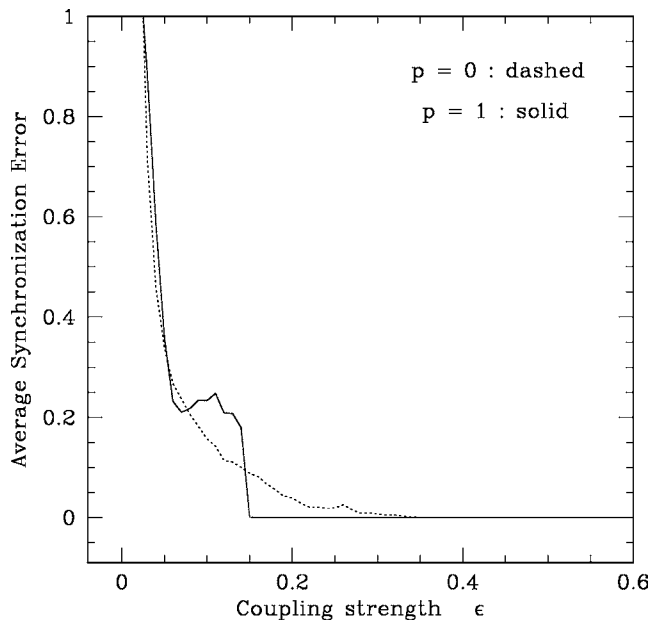


FIG. 4. Average synchronization error vs coupling strength ϵ , for rewiring probability (i) $p=0$ (fully regular) and (ii) $p=1$ (fully random). Clearly the fully random network achieves zero synchronization error at a much smaller value of coupling strength, and hence gives rise to a larger range of synchronization in coupling parameter space.

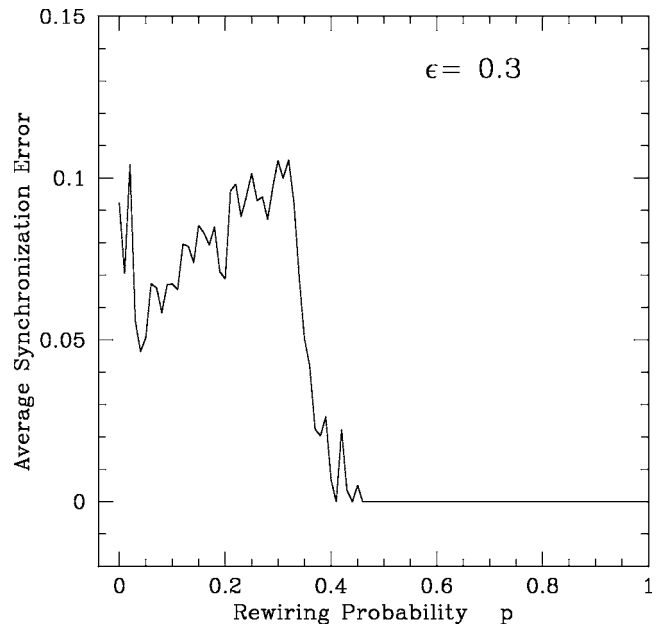


FIG. 5. Average synchronization error vs rewiring probability p , for the network of model neurons with coupling strength $\epsilon=0.3$.

with appropriate strength, as every site interacts with all other sites over a period of time. Taking a clue from the law of large numbers, we conjecture that the total contribution due to k randomly chosen neighbors is $k\langle x(t) \rangle$, where $\langle x(t) \rangle$ is the mean value of x . So the dynamics can be mimicked well by an averaged evolution equation [see Eq. (B1) of Appendix B]. The spatiotemporal fixed point obtained from such an effective time-averaged system is exactly the same as that from our randomly rewired network. The results are also markedly similar for the range of spatial synchronization for

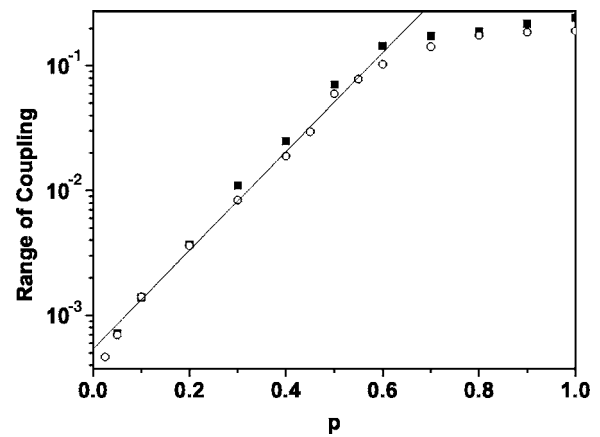


FIG. 6. Continuous range of coupling ϵ over which synchronization is observed, plotted as a function of the rewiring probability p , on a semilogarithmic scale (circles). Note that in this synchronized regime the fixed point solution is unstable and we get synchronized chaos or synchronized oscillations. We carry out simulations for network size $N=500$, averaging over 10 configurations, to find the continuous parameter range over which synchronization is obtained. For smaller p , we clearly see an exponential growth. Also shown is data for the same quantity obtained via Eq. (B1) (black squares).

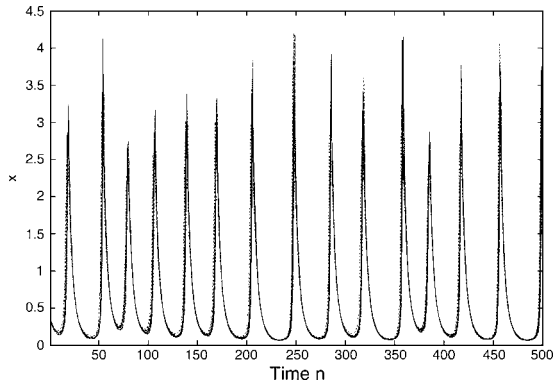


FIG. 7. Time trace of 10 neurons superposed in a network of nonidentical neurons. In this figure the strength of parametric fluctuations were 0.005 for parameters a , b , and c , and 0.001 for parameter k (approximately up to 1% of the parameter value for all four parameters). Clearly, though complete synchronization is lost due to inhomogeneity, the neurons are still phase synchronized.

the two cases (see Fig. 6). Further we can use this mean-field analogue to obtain good analytical estimates of the coupling range (see details in the appendix).

IV. NETWORK OF NONIDENTICAL NEURONS

Now we consider the network of nonidentical neurons, with a spread in the individual values of the parameters: a, b, c, k . It is evident from the neuronal time traces displayed in Fig. 7 that such inhomogeneity has a very small effect on the synchronization properties of the network. In fact, synchronization is surprisingly robust to parametric noise in its individual neuronal components.

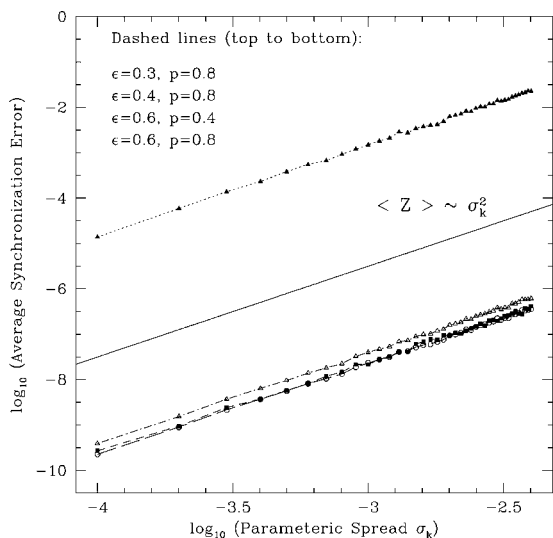


FIG. 8. Average synchronization error $\langle Z \rangle$ vs parametric noise strength σ_k (up to 10% of the parameter value), for four different sets of coupling strength ϵ and rewiring probability p . The top set belongs to the synchronized chaos phase, while the bottom three lie in the spatiotemporal fixed point phase. Here $N=50$ (but note that system size makes no discernible difference to the average synchronization error). The case of $\sigma_k=0$ yields $\langle Z \rangle=0$.

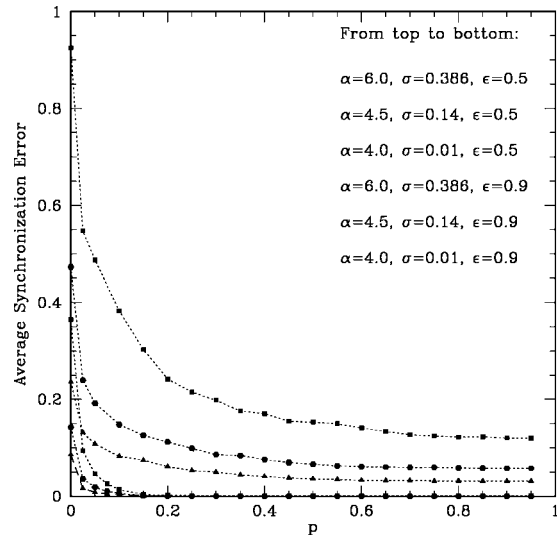


FIG. 9. Average synchronization error vs rewiring probability p , for the network of model Rulkov neurons with coupling strengths $\epsilon=0.5, 0.9$, for parameter sets (i) $\alpha=4.0, \sigma=0.01$, (ii) $\alpha=4.5, \sigma=0.14$, and (iii) $\alpha=6, \sigma=0.386$. These parameter sets include both spiking and spiking-bursting regimes of neuronal activity.

In particular, consider a spread of σ_k in the parameter k . The resulting average synchronization error increases with increasing strength of parametric noise, namely increasing network inhomogeneity, as a power law,

$$\langle Z \rangle \sim \sigma_k^2, \tag{9}$$

where $\langle Z \rangle$ is $Z(n)$ [defined by Eq. (8)] averaged over time and over a large number of network realizations. Note that the average synchronization error is very small (of the order of $\sim 10^{-8}$) even when the spread in parameters is as large as 10% of the parameter value (see Fig. 8) [18].

The σ_k^2 dependence of the synchronization error in the spatiotemporal fixed point regime can be rationalized from the fact that $\langle Z \rangle$ [from Eq. (8)] approximately varies as

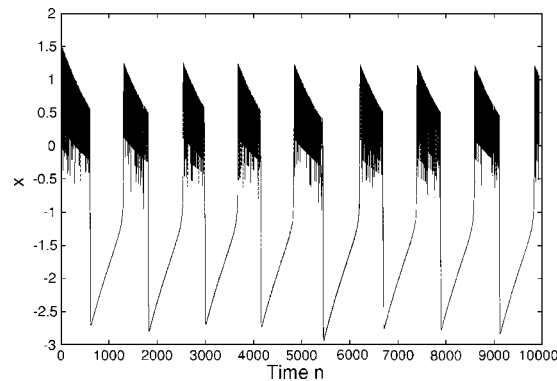


FIG. 10. Representative wave forms of 10 neurons superposed in a network of model Rulkov neurons with coupling strengths $\epsilon=0.5$, and $\alpha=4.5, \sigma=0.14$. It is clear that the bursting pattern of all the neurons is perfectly in-phase, while the amplitudes are not exactly matched.

$(\Delta x_i^*)^2$ where Δx_i^* is the variation in the fixed points of the individual neuronal maps. Since, from Eq. (2), this variation goes as $\sigma_k, \langle Z \rangle \sim \sigma_k^2$. This indicates that the source of synchronization error in the spatiotemporal fixed point regime in the network of heterogeneous components, arises only from the variation in the fixed points of the nonidentical individual maps.

Computing the average synchronization error with respect to noise in the other parameters, a , b , and c , also yields a relationship like Eq. (9). Note that the Newton-Raphson solution of Eqs. (2) and (5) show that the variation in the fixed point of the system also has a linear relation with variation in parameters a , b or c (just as in the more obvious case of parameter k).

V. NETWORK OF MODEL RULKOV NEURONS

In order to check the generality of the qualitative results, we now briefly consider a network comprised of neurons described by a different model: the Rulkov map. This model of neurons replicates both the spiking and spiking-bursting activity of neurons. We will again show that increasing randomness in coupling connections in this network enhances synchronization.

Specifically, the local dynamical unit now is the two-dimensional model neuron map proposed by Rulkov [12]. It is given in discrete time n as

$$\begin{aligned} x_{n+1} &= f(x_n, y_n + \beta), \\ y_{n+1} &= y_n - \mu(x_n + 1) + \mu\sigma. \end{aligned} \quad (10)$$

The x_n is the fast and y_n is the slow dynamical variable. The slow evolution of y_n arises from small values of parameter $\mu=0.001$. The function $f(x, y)$ is discontinuous, and is given by

$$\begin{aligned} f(x, y) &= \alpha/(1-x) + y \quad \text{when } x \leq 0, \\ f(x, y) &= \alpha + y \quad \text{when } 0 < x < \alpha + y, \\ f(x, y) &= 1 \quad \text{when } x \geq \alpha + y, \end{aligned} \quad (11)$$

where α is the control parameter of the map.

Figure 9 shows the synchronization error as a function of the degree of disorder p of the underlying network. Depending on the activity patterns of the individual neurons, the network goes to a spatiotemporal fixed point (e.g., at $\alpha=4$, $\sigma=-0.01$), or to a completely synchronized or a phase synchronized state [19] (see Fig. 10). It is generally observed that the average synchronization error monotonically decreases with increasing p . This behavior is observed for many different regimes and for many different individual activity patterns occurring at varying time scales, including both spiking and bursting, as is evident from the representative examples in Fig. 9.

VI. CONCLUSIONS

We have studied the spatiotemporal dynamics of a network of model neurons, under variation of coupling strength ϵ and degree of randomness in coupling p . We find that at

high coupling strengths ($\epsilon > \epsilon_{\text{fixed}}$) the unstable saddle point solution of the local chaotic maps gets stabilized. The range of coupling where this spatiotemporal fixed point gains stability is unchanged in the presence of randomness in the connections, namely ϵ_{fixed} is invariant under changes in p . As coupling gets weaker ($\epsilon < \epsilon_{\text{fixed}}$), the spatiotemporal fixed point loses stability, and one obtains chaos. In this regime, when the coupling connections are completely regular ($p=0$), the network becomes spatiotemporally chaotic. Interestingly however, in the presence of random links ($p > 0$) one obtains spatial synchronization in the network.

We have demonstrated that synchronization properties, such as the range of synchronized chaos, increases *exponentially* with the fraction of random links in the network, up to (nearly) completely random networks. So we find no evidence of synchronization peaking or saturating at dilute random rewiring (that is, small world networks do not show enhanced or optimal synchronization effects).

Further we find that in the space of fixed coupling strengths, the synchronization transition occurs at a *finite* value of p . So here long-range order is obtained at a finite degree of disorder in coupling connections, unlike expectations from models where one obtains long-range order even at infinitesimal rewiring probability in the infinite size limit.

Finally, in order to check the generality and reach of our observations, we have investigated networks of nonidentical neurons, as well as networks of neurons displaying both spiking and bursting dynamics. Both these studies clearly show that random rewiring does indeed enhance synchronization, even in networks with inhomogeneous components, as well as in networks where the nodal dynamics has multiple time scales such as spiking-bursting.

ACKNOWLEDGMENTS

The first two authors (M.P.K.J. and A.R.S.) would like to thank the Complex Systems School (organized in the Institute of Mathematical Sciences in collaboration with Santa Fe Institute), where this project was initiated. The authors would also like to thank Sitabhra Sinha for many stimulating discussions on the subject. Further one of the authors (A.R.S.) would like to thank the PU-BARC programme for support.

APPENDIX A: STABILITY ANALYSIS OF $p=0$

Now we analyze the stability of synchronized fixed point for regular nearest neighbor coupling topology, i.e., the $p=0$ case whose evolution is given by Eq. (6).

For the homogenous solution of Eq. (6), the stability criterion is that the norm of eigenvalues of $2N \times 2N$ stability matrix J have magnitude less than unity. The onset of synchronization is characterized by the crossover of eigenvalues past unity for different coupling strength ϵ . The Jacobian matrix J for the synchronized fixed point for the $2N$ -dimensional system is given by

$$\mathbf{J} = \begin{pmatrix} (1-\epsilon)a_1 & (1-\epsilon)a_2 & \frac{\epsilon}{2} & 0 & 0 & 0 & \dots & \frac{\epsilon}{2} & 0 \\ a_3 & a_4 & 0 & 0 & 0 & 0 & \dots & 0 & 0 \\ \frac{\epsilon}{2} & 0 & (1-\epsilon)a_1 & (1-\epsilon)a_2 & \frac{\epsilon}{2} & 0 & \dots & 0 & 0 \\ 0 & 0 & a_3 & a_4 & 0 & 0 & \dots & 0 & 0 \\ \vdots & \vdots & \vdots & \vdots & \vdots & \vdots & \ddots & \vdots & \vdots \\ \frac{\epsilon}{2} & 0 & 0 & 0 & 0 & 0 & \dots & (1-\epsilon)a_1 & (1-\epsilon)a_2 \\ 0 & 0 & 0 & 0 & 0 & 0 & \dots & a_3 & a_4 \end{pmatrix},$$

where

$$a_1 = \frac{\partial f_1(x,y)}{\partial x} = 2x^* \exp(y^* - x^*) - x^{*2} \exp(y^* - x^*),$$

$$a_2 = \frac{\partial f_1(x,y)}{\partial y} = x^{*2} \exp(y^* - x^*),$$

$$a_3 = \frac{\partial f_2(x,y)}{\partial x} = -b,$$

$$a_4 = \frac{\partial f_2(x,y)}{\partial y} = a. \tag{A1}$$

The above values are $a_1 = 1.004\ 358 \pm (0.000\ 002)$ and $a_2 = 0.933\ 357 \pm (0.000\ 002)$. In principle, x^* and y^* are functions of ϵ . However they turn out to be very slowly varying functions. (Using feedback to stabilize the fixed point in its unstable range, we tracked down the values of x^* and y^* over the entire range of ϵ .) The values of a_1 and a_2 hardly change over this range and error bars are given above. The general form of the above matrix is

$$\mathbf{J} = \begin{pmatrix} A & B & 0 & \dots & B \\ B & A & B & \dots & 0 \\ \vdots & \vdots & \vdots & \ddots & \vdots \\ B & 0 & 0 & \dots & A \end{pmatrix}.$$

The matrix J is block circulant matrix, where each block is 2×2 matrix, where

$$\mathbf{A} = \begin{pmatrix} (1-\epsilon)a_1 & (1-\epsilon)a_2 \\ a_3 & a_4 \end{pmatrix}, \quad \mathbf{B} = \begin{pmatrix} \frac{\epsilon}{2} & 0 \\ 0 & 0 \end{pmatrix},$$

A block circulant matrix can be set into a block-diagonal form by a unitary transformation. The unitary matrix which affects the block diagonalization is a direct product of Fourier matrices of sizes $N \times N$ and 2×2 , the entries of which are roots of unity, independent of the matrix being diagonalized [20,21].

The block diagonal form is

$$\mathbf{D} = \begin{pmatrix} M_0 & 0 & \dots & 0 \\ 0 & M_1 & \dots & 0 \\ \vdots & \vdots & \ddots & \vdots \\ 0 & 0 & \dots & M_{N-1} \end{pmatrix},$$

where the matrix, M_r ; $r=0,1,2,\dots,N-1$ are 2×2 matrices given as $M_r = A + \omega_r B + \omega_r^{N-1} B$, $\omega_r = e^{i\theta}$ and $\omega_r^{N-1} = e^{-i\theta}$, $\theta_r = 2\pi r/N$,

$$\mathbf{M}_r = \begin{pmatrix} (1-\epsilon)a_1 + \epsilon \cos \theta_r & (1-\epsilon)a_2 \\ a_3 & a_4 \end{pmatrix} \tag{A2}$$

and, for $r=0$, the matrix is

$$\mathbf{M}_0 = \begin{pmatrix} (1-\epsilon)a_1 + \epsilon & (1-\epsilon)a_2 \\ a_3 & a_4 \end{pmatrix}. \tag{A3}$$

Now it is evident that one must check the eigenvalues of M for θ_r between 0 to 2π to obtain the stability criterion for all values of N . Actually, it is sufficient to check for $0 \leq \theta_r \leq \pi$. Eigenvalues of the stability matrix could be real or complex. First we consider the case of real eigenvalues and check if their absolute value ever exceeds unity. We consider the matrices $S_{\pm} = (M \pm I)$. The eigenvalues of these matrices are simply the eigenvalues of M shifted by ± 1 . Now if eigenvalues of S_+ are positive and eigenvalues of S_- are negative, the eigenvalues of M must be bounded between $[-1, 1]$. (We drop the subscript r for simplicity.)

Consider the determinant of matrix S_+ , $\det S_+ = (a_4 + 1) \times [(1-\epsilon)a_1 + (\epsilon \cos \theta_r + 1)] - a_2 a_3 (1-\epsilon)$. We see that the determinant is always positive for any value of θ as $[1 + \epsilon \cos(\theta_r)]$ will always be positive since $\epsilon < 1$. Let us consider matrix S_- . Its determinant is $\det S_- = (a_4 - 1)[(1-\epsilon)a_1 + \epsilon \cos \theta_r - 1] - a_2 a_3 (1-\epsilon)$. It is also positive as the last term is positive and is greater than the first term.

Similarly, $\text{Tr } S_+ = (1-\epsilon)a_1 + \epsilon \cos \theta_r + a_4 + 2 = (a_1 + a_4 + 2) + \epsilon(\cos \theta_r - a_1)$, which is also positive for both $\theta_r = 0$ and $\theta_r = \pi$. So, the eigenvalues of the matrix S_+ are positive. Now the trace of matrix S_- is given by $\text{Tr } S_- = (1-\epsilon)a_1 + \epsilon \cos \theta_r + a_4 - 2 = (a_1 + a_4 - 2) + \epsilon(\cos \theta_r - a_1)$. Since $(a_1 + a_4 - 2)$ and $[\cos(\theta_r) - a_1]$ are negative for all θ_r , the trace of the matrix S_-

is negative. Thus the eigenvalues of this matrix must be negative. This implies that the real eigenvalues are within the interval $[-1, 1]$.

Now consider the possibility of complex eigenvalues. In this case, the stability criterion is that the norms of the eigenvalues are less than unity. (Or alternatively, square of the norm is less than unity.) For a two-dimensional matrix, the square of the norm of the eigenvalues is the same as determinant of the matrix. Now considering the determinant of the matrix equal to unity to find the ϵ where synchronized fixed point becomes stable, we have

$$\det M_r = (1 - \epsilon)a_1a_4 + a_4\epsilon \cos \theta_r - a_3a_2(1 - \epsilon) = 1 \quad (\text{A4})$$

then, $\epsilon = 1 - (a_1a_4 - a_2a_3)/a_4 \cos \theta_r - (a_1a_4 - a_2a_3) = (1 - z_1)/(a_4 \cos \theta_r - z_1)$, where $z_1 = 1.0618$. Thus the maximum value of ϵ is obtained for $\theta_r = 0$, i.e., $\epsilon_{\text{fixed}} \sim 0.36$. Second, it is easily seen that the eigenvalues are always complex for the full range of ϵ for $\theta_r = 0$. The determinant is a decreasing function of ϵ for a given $\cos(\theta_r)$ and an increasing function of $\cos(\theta_r)$ for a given ϵ . Thus the maximum value of ϵ above which stability is guaranteed is the same as the bound obtained for M_0 , i.e., if $\epsilon > \epsilon_{\text{fixed}}$. This is in agreement with the numerical results (see Fig. 1).

APPENDIX B: STABILITY ANALYSIS FOR FINITE p

Stability analysis for finite p is relatively complicated even for the synchronous fixed point since it will involve diagonalization of random matrices which are not in a known class.

We employ an approximation similar to that employed by Pandit and Amritkar [22] while studying random walks on a small-world network. They treated the random part as a kind of global coupling with appropriate strength and they get results which are comparable to ones numerically obtained. Taking a clue from the law of large numbers, we conjecture that the total contribution due to k randomly chosen neighbors is $k\langle x(t) \rangle$. Now the averaged out evolution equation could be written as

$$\begin{aligned} x_{n+1}(i) &= (1 - \epsilon)f_1[x_n(i), y_n(i)] + (1 - p)\frac{\epsilon}{2}\{g[x_n(i+1)] \\ &+ g[x_n(i-1)]\} + \frac{\epsilon p}{N} \sum_{i=1}^N \{g[x_n(i)]\}, \\ y_{n+1}(i) &= f_2[x_n(i), y_n(i)]. \end{aligned} \quad (\text{B1})$$

The Jacobian matrix J' , for a two-dimensional map with random rewired network is given by

$$J' = \begin{pmatrix} (1 - \epsilon)a_1 + \frac{\epsilon p}{N} & (1 - \epsilon)a_2 & (1 - p)\frac{\epsilon}{2} + \frac{\epsilon p}{N} & 0 & \dots & (1 - p)\frac{\epsilon}{2} + \frac{\epsilon p}{N} & 0 \\ a_3 & a_4 & 0 & 0 & \dots & 0 & 0 \\ (1 - p)\frac{\epsilon}{2} + \frac{\epsilon p}{N} & 0 & (1 - \epsilon)a_1 + \frac{\epsilon p}{N} & (1 - \epsilon)a_2 & \dots & \frac{\epsilon p}{N} & 0 \\ 0 & 0 & a_3 & a_4 & \dots & 0 & 0 \\ \vdots & \vdots & \vdots & \vdots & \ddots & \vdots & \vdots \\ (1 - p)\frac{\epsilon}{2} + \frac{\epsilon p}{N} & 0 & \frac{\epsilon p}{N} & 0 & \dots & (1 - \epsilon)a_1 + \frac{\epsilon p}{N} & (1 - \epsilon)a_2 \\ 0 & 0 & 0 & 0 & \dots & a_3 & a_4 \end{pmatrix},$$

where, the values of constants a_1, a_2, a_3, a_4 are the same as in Eq. (A1).

The matrix J' is a block circulant matrix, where each block is a 2×2 matrix. The unitary matrix which affects block diagonalization of the block circulant matrix is a direct product of Fourier matrices of sizes $N \times N$ and 2×2 , the entries of which are roots of unity, independent of the matrix being diagonalized [20,21]. The general form of the block circulant Jacobian here is

$$J' = \begin{pmatrix} A' + C' & B' + C' & C' & C' & \dots & C' & B' + C' \\ B' + C' & A' + C' & B' + C' & C' & \dots & C' & C' \\ \vdots & \vdots & \vdots & \vdots & \ddots & \vdots & \vdots \\ B' + C' & C' & C' & C' & \dots & B' + C' & A' + C' \end{pmatrix},$$

where

$$A' = \begin{pmatrix} (1 - \epsilon)a_1 & (1 - \epsilon)a_2 \\ a_3 & a_4 \end{pmatrix}, \quad B' = \begin{pmatrix} (1 - p)\frac{\epsilon}{2} & 0 \\ 0 & 0 \end{pmatrix}, \quad C' = \begin{pmatrix} \frac{\epsilon p}{N} & 0 \\ 0 & 0 \end{pmatrix}.$$

The block diagonal form is

$$\mathbf{D}' = \begin{pmatrix} M'_0 & 0 & \dots & 0 \\ 0 & M'_1 & \dots & 0 \\ \vdots & \vdots & \ddots & \vdots \\ 0 & 0 & \dots & M'_{N-1} \end{pmatrix},$$

where the matrix M'_r ; $r=0,1,2,\dots,N-1$ are 2×2 matrices given as, $M'_r = (A' + C') + \omega_r(B' + C') + \omega_r^2 C' + \dots + \omega_r^{N-1}(B' + C')$, where, $\omega_r = e^{i\theta_r}$ and $\omega_r^{N-1} = e^{-i\theta_r}$, $\theta_r = 2\pi r/N$. Therefore, $M'_r = A' + B'(e^{i\theta_r} + e^{-i\theta_r}) + C'(1 + e^{i\theta_r} + e^{2i\theta_r} + \dots + e^{(N-1)i\theta_r}) = A' + 2B' \cos \theta_r + C'(1 + e^{i\theta_r} + e^{2i\theta_r} + \dots + e^{(N-1)i\theta_r})$.

Here we must to consider two cases, viz. $\theta_r=0$ and $\theta_r \neq 0$. In the first case, it is easily checked that the form of the matrix $M'_r = A' + 2B' + NC'$ is exactly the same as that obtained for the $p=0$ case in the preceding appendix, i.e.,

$$\mathbf{M}'_0 = \begin{pmatrix} (1-\epsilon)a_1 + \epsilon & (1-\epsilon)a_2 \\ a_3 & a_4 \end{pmatrix}. \quad (\text{B2})$$

The eigenvalues are both real and complex, and synchronization is obtained at $\epsilon \geq \epsilon_{\text{fixed}}$, as observed numerically as well.

For the $r \neq 0$ case, the matrix is slightly different and is given as $M'_r = A' + 2B' \cos \theta_r$,

$$\mathbf{M}'_r = \begin{pmatrix} (1-\epsilon)a_1 + \epsilon(1-p)\cos \theta_r & (1-\epsilon)a_2 \\ a_3 & a_4 \end{pmatrix}. \quad (\text{B3})$$

As previously mentioned, one checks the eigenvalues of M'_r for $\cos(\theta_r)$ between -1 to 1 (or equivalently θ_r between 0 to π). We note that $\theta_1 \rightarrow 0$ in the thermodynamic limit N

$\rightarrow \infty$. Eigenvalues of the stability matrix could be real or complex. We again consider the matrix $S'_\pm = (M' \pm I)$. Now, the determinant of matrix S'_+ is, $\det S'_+ = (a_4 + 1)\{(1-\epsilon)a_1 + [1 + (1-p)\epsilon \cos \theta_r]\} + [-a_2 a_3(1-\epsilon)]$. We see that determinant is always positive for extremum values of $\theta_r=0, \pi$, since all the terms are positive. Similarly, for matrix S'_- , $\det S'_- = (a_4 - 1)\{(1-\epsilon)a_1 + [(1-p)\epsilon \cos \theta_r - 1]\} + [-a_2 a_3(1-\epsilon)]$. Here the determinant is positive because the product of the curly brackets is positive. The trace of matrix S'_+ is $\text{Tr } S'_+ = [(1-\epsilon)a_1 + a_4] + [2 + \epsilon(1-p)\cos \theta_r]$. It is positive due to the fact that both the brackets are positive for both $\theta_r=0, \pi$. But the trace of matrix S'_- is $\text{Tr } S'_- = [(1-\epsilon)a_1 + a_4] + \epsilon(1-p)\cos \theta_r - 2 = (a_1 + a_4 - 2) + \epsilon[(1-p)\cos \theta_r - a_1]$. Since $a_1 + a_4 - 2$ and $[(1-p)\cos(\theta_r - a_1)]$ are both negative, $\text{Tr } S'_-$ is negative. Thus we can say that the eigenvalues of matrix M'_r , if real, are within interval $[-1, 1]$. Now in the case of complex eigenvalues there are two bounds $\theta_r=0$ and $\theta_r=\pi$. We can see that at finite p , the case for $\theta_r=0$ is the same as in $p=0$. The determinant of matrix M' is

$$\det M'_r = [(1-\epsilon)a_1 + \epsilon \cos \theta_r(1-p)]a_4 - a_2 a_3(1-\epsilon). \quad (\text{B4})$$

Comparing $\det M'_r$ in Eq. (B4) with $\det M_r$ in Eq. (A4), we observe that $\det M'_r \leq \det M_r \leq \det M'_0$ for $\cos(\theta_r) > 0$. Since $M_0 = M'_0$, stability is guaranteed for $\epsilon > 0.36$ for any value of p . For $\cos(\theta_r) < 0$ the maximum value of determinant is reached for $\theta_r = \pi$ and $p=1$ and in that case, the determinant does not exceed unity for $\epsilon > 0.05$. It can be easily seen that the determinant is a decreasing function of ϵ . So we can conclude that the range of the synchronized fixed point remains at ϵ_{fixed} even at finite p . This is in complete agreement with the numerics presented in this work.

-
- [1] *Theory and Applications of Coupled Map Lattices*, edited by K. Kaneko (Wiley, New York, 1993), and references therein.
 [2] For instance, see examples, in K. Kaneko, Phys. Rev. Lett. **65**, 1391 (1990); G. Perez, S. Sinha, and H. A. Cerdeira, Physica D **63**, 341 (1993).
 [3] D. J. Watts and Strogatz Nature (London) **393**, 440 (1998); J J Collins and C C Chow *ibid.* **393**, 409 (1998).
 [4] J. J. Hopfield and A. V. M. Hertz, Proc. Natl. Acad. Sci. U.S.A. **92**, 6655 (1995).
 [5] P. M. Gade and C. K. Hu, Phys. Rev. E **62**, 6409 (2000).
 [6] S. A. Pandit and R. E. Amritkar, Phys. Rev. E **60**, R1119 (1999).
 [7] M. Barthelemy and Luis A. Nunes Amaral, Phys. Rev. Lett. **82**, 3180 (1999).
 [8] A. Pikovsky, M. Rosenblum, and J. Kurths, *Synchronization: A Universal Concept in Nonlinear Sciences* (Cambridge University Press, Cambridge, 2001).
 [9] S. Sinha, Phys. Rev. E **66**, 016209 (2002).
 [10] The effects of random connections on the emergence of collective behaviors other than synchronization have also been investigated in coupled map networks; for example, in co-evolving dynamics [such as P. Gong and C. van Leeuwen, Europhys. Lett. **67**, 328 (2004)]; in turbulence [such as M. G.

- Cosenza and K. Tucci Phys. Rev. E **65**, 036223 (2002)]; in epilepsy [such as T. I. Netloff *et al.*, J. Neuroscience **24**, 8075 (2004)].
 [11] D. R. Chialvo, Chaos, Solitons Fractals **5**, 461 (1995).
 [12] N. F. Rulkov, Phys. Rev. E **65**, 041922 (2002).
 [13] C. Bonatto, J. C. Garreau, and J. A. C. Gallas, Phys. Rev. Lett. **95**, 143905 (2005).
 [14] It has been suggested for certain cases that small world connectivity (namely very small p) gives something special which is amiss in regular or random lattices, leading to a conjecture that small world connections yield special dynamical features that are absent in both the regular and the random limits. For instance, see L. F. Lago-Fernandez, R. Huerta, F. Corbacho, and J. A. Siguenza, Phys. Rev. Lett. **84**, 2758 (2000).
 [15] Other connection schemes are indeed possible as well, such as one where the connectivity varies with the distance between sites as a power law. See, e.g., S. Raghavachari and J. A. Glazier, Phys. Rev. Lett. **74**, 3297 (1995). Investigations of such networks would be of considerable interest as well.
 [16] In the phase diagram we show the continuous range of ϵ values over which spatial synchronization is seen. Very close to this range, we have a very small parameter regime which shows

both synchronized and unsynchronized states. Since it is rather narrow, it is not shown in phase diagram.

[17] P. M. Gade and S. Sinha, Phys. Rev. E **72**, 052903 (2005).

[18] Note that noise in the variables of the local maps also degrades synchronization, though within some noise level this increase in synchronization error is quite minimal. For instance, typically, for noise levels up to 1% of the maximum value of the variable, the synchronization error is increased by less than 0.1%. The average error though increases more rapidly under noise levels stronger than 5% or so.

[19] M. V. Ivanchenko, G. V. Osipov, V. D. Shalfeev, and J. Kurths Phys. Rev. Lett. **93**, 134101 (2004); N. F. Rulkov, *ibid.* **86**, 183 (2001); I. Belykh, E. de Lange, and M. Hasler, *ibid.* **94**, 188101 (2005).

[20] P. J. Davis, *Circulant Matrices* (Wiley, New York, 1979).

[21] P. M. Gade and R. E. Amritkar, Phys. Rev. E **47**, 143 (1993).

[22] S. A. Pandit and R. E. Amritkar, Phys. Rev. E **63**, 041104 (2001).